ASTFE American Society of Thermal and Fluids Engineers

Proceedings of the 2nd Thermal and Fluid Engineering Conference, TFEC2017
4th International Workshop on Heat Transfer, IWHT2017
April 2-5, 2017, Las Vegas, NV, USA

TFEC-IWHT2017-16865

THERMAL RESISTANCE NETWORK MODEL FOR HEAT PIPE – PCM BASED COOL STORAGE SYSTEM

Sean Hoenig[1*], CJ Pan[2], Chien-Hua Chen[1], and Richard Bonner III[1]

[1]Advanced Cooling Technologies, Inc., Lancaster, PA 17601, USA
[2]Lehigh University, Bethlehem, PA 18015, USA

ABSTRACT

A robust system configuration is determined to design and integrate an innovative heat pipe – PCM based cool storage system as supplemental dry cooling for air cooled condensers. Due to the complexity of the full scale system, a unique thermal resistance network model is developed to determine the thermal performance and overall capital cost for optimization of component design parameters. The development of this design tool is necessary to obtain practical thermal performance and capital cost information below \$150/kW_{th} given an energy storage capacity requirement. To enable this analysis, transient numerical modeling using fundamental thermal resistance calculations and thermosyphon dynamics was implemented. Validation of the numerical model is done through a system comparison with ANSYS Fluent. Optimization results through parametric studies have demonstrated applicable designs capable for effective heat transfer utilization into and out of the phase change material and within cost constraints. Given a target energy storage capacity goal, optimal sizing trends of design parameters is determined. The influence of thermosyphon and fin sizing and number on system performance has been demonstrated as critical parameters in overall system configuration.

KEY WORDS: thermal resistance network, numerical modeling, parametric studies, heat pipe heat exchanger, phase change material energy storage

1. INTRODUCTION

Advanced cooling technologies for effective thermal dissipation of low grade heat dictate the future of the electric power industry. These technologies are especially important for power plant operation where a constrained supply of useable water continues to shrink. In the ARPA-e ARID Program, transformative power plant cooling technologies were sought "that enable high thermal-to-electric energy conversion efficiency with zero net water dissipation to the atmosphere" [1]. To understand this necessity, it is important to define the differences in wet and dry cooling. Wet cooling utilizes large bodies of fresh water in once-through or wet-recirculating systems for effective steam condensation. Dry cooling relies on the convective heat transfer from steam to air without direct contact for effective cooling. This is typically seen through the use of air cooled condenser (ACC) systems, which only comprise 1% of the electric power generation market [2]. A shift towards dry cooling technologies in thermoelectric generation would help meet growing demands for fresh water in other sectors of society.

With respect to the ARPA-e ARID Program, Advanced Cooling Technologies, Inc. proposed an innovative supplemental cool storage system that utilizes an integrated heat pipe-phase change material (PCM) heat exchanger to transfer heat from the steam into a PCM reservoir during an operational cycle. The stored heat is then rejected at night to the cooler ambient air, resolidifying the PCM. An example of the proposed concept design can be seen below in Figure 1. Figure 2 then demonstrates how this technology would function within a typical power generation steam cycle. An important difference to note is that while ACC's are direct dry cooling systems where fans blow air directly along steam bundle for convective condensation, additional technologies utilize indirect dry cooling. This method uses air as a secondary cooling medium,

*Corresponding Author: Sean.Hoenig@1-ACT.com

where cooling water flows in a closed heat exchanger system with the steam bundle and never contacts the cooling air [3]. The proposed technology can be suitable for both applications. For this project, major research areas include but are not limited to identification and utilization of a suitable phase change material, effective thermosyphon design and manufacturability with a modular PCM heat sink, and precise thermal performance and cost analysis capabilities.

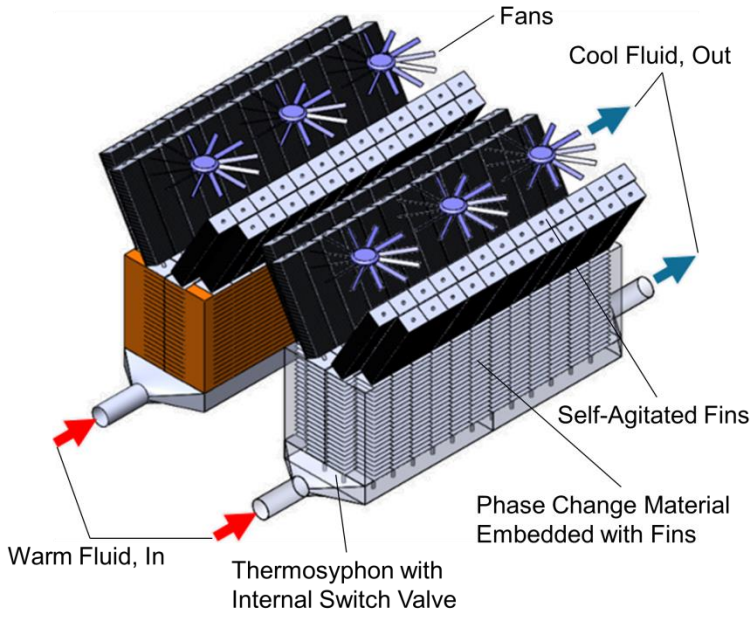

Fig. 1 The concept design for a heat pipe-PCM heat exchanger system.

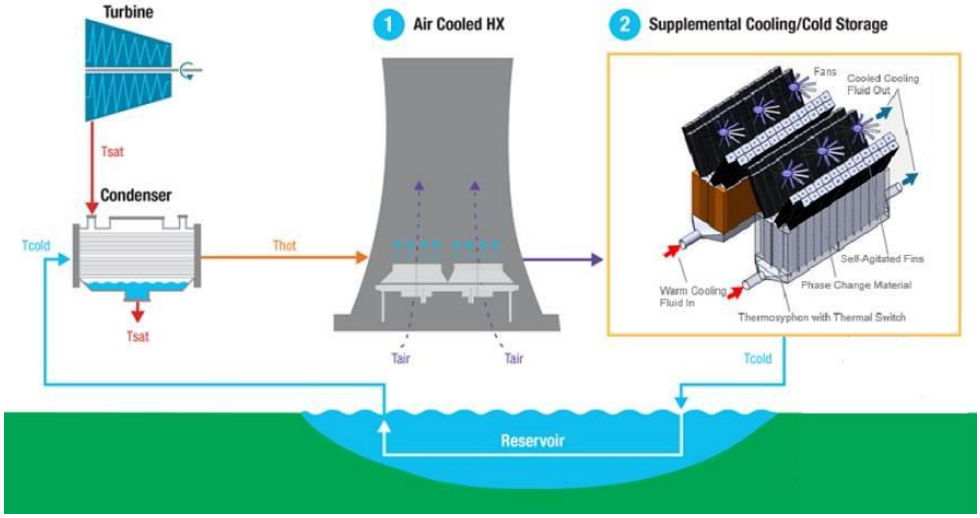

Fig. 2 Supplemental dry cooling for the proposed cool storage system.

To properly model the thermal performance and obtain practical capital cost analysis of the full scale system, a transient numerical based thermal resistance network (TRN) model was developed. This is done to ultimately gain insight into the optimization of component design parameters. It was determined early on that a detailed CFD based model will be very challenging to complete for the specific design goals in a timely fashion. An Excel-based design tool can sufficiently demonstrate the thermal capabilities and overall capital cost below \$150/kW_{th} to demonstrate the technology's value proposition. To implement this analysis, fundamental thermal resistance calculations and thermosyphon dynamics were used to create a transient forward-difference numerical model. Parametric studies are then used to optimize the sizing of component design parameters given a target energy storage capacity.

2. MODEL CONFIGURATION

To predict the thermal performance of the cool storage system, the thermal resistance network model was developed to determine the transient temperature history through each component section. This forward-difference numerical analysis determines the PCM melt time for a given system sizing. An initial understanding of the critical thermal resistance pathways involved in effective heat transfer from inlet cooling water to PCM can be seen below in Figure 3. This graphic is used to demonstrate the overall equivalent thermal resistances of the cool storage system. Nodal analysis was completed to determine the principal node temperatures over time. Figure 4 is a representative experimental module structure that identifies the physical structures of the setup. A summary and definition of the major thermal resistances mentioned below can be seen in Table 1.

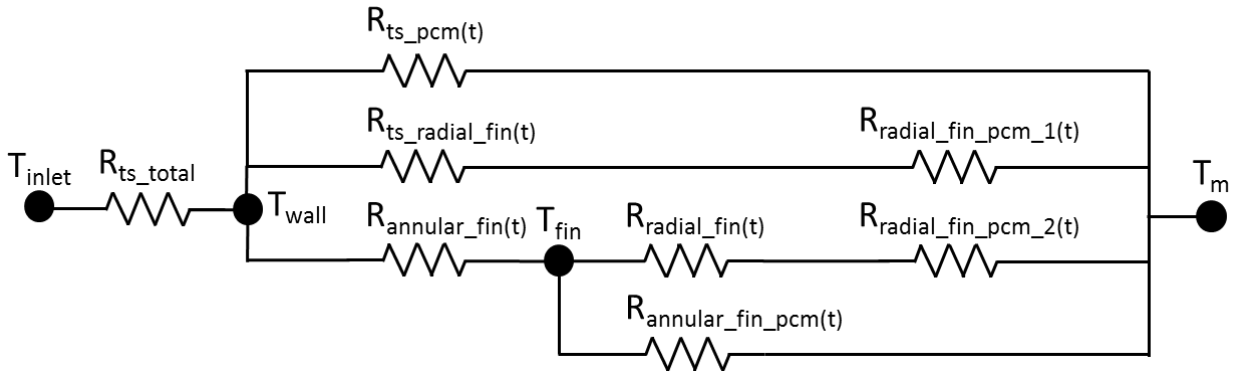

Fig. 3 Intricate series-parallel resistance network for the entire system module.

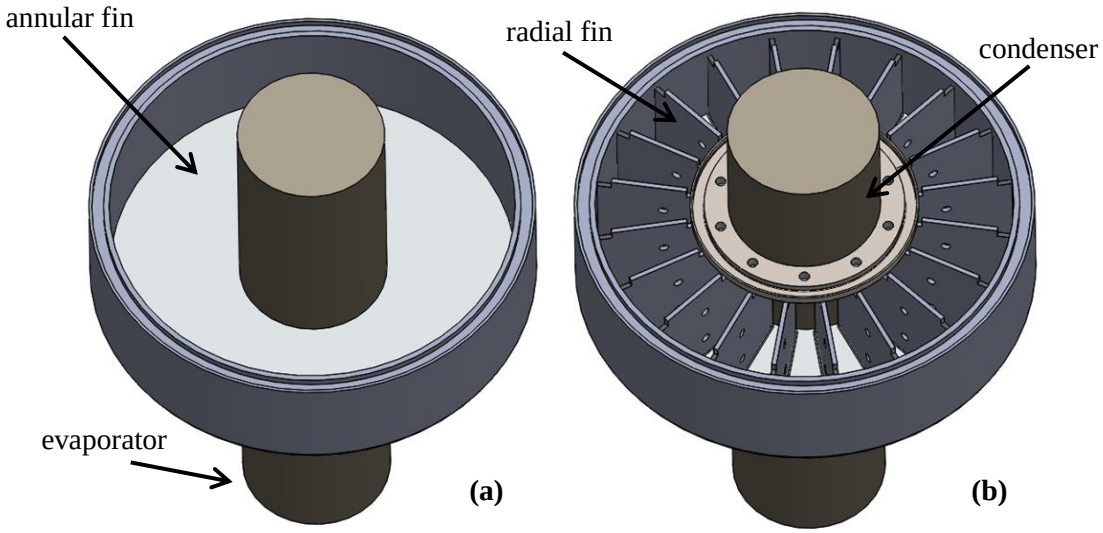

Fig. 4 SolidWorks model of a geometric arrangement for the fin-PCM module. Image (a) is without radial fins while image (b) includes radial fins inside the module structure.

In this model, a complex resistance network is used in the calculations. This is exemplified by the configuration in Figure 3 and graphically depicted below in Figure 5. The total thermosyphon resistance is comprised of five subsequent resistance values (R_{wall}, $R_{evaporator}$, R_{vapor_space}, $R_{condenser}$, R_{wall}) in series while the fin-PCM module is an intricate series-parallel resistance construct. While the thermosyphon resistance is constant, the fin-PCM module resistances vary throughout the phase change process. This is due to the changing characteristic length of the PCM melt front. While the thermosyphon resistances are standard in derivation, a unique aspect of this configuration is that a fin efficiency method is used to account for the changing Biot number as the PCM melts. These temperature distributions are empirically derived to account for the changing heat transfer efficiency. The primary reason this is done is to account for the fact that normally the thermal resistance of a fin structure is

founded on a two-dimensional heat transfer assumption [4]. In other words, due to the changing temperature gradients developed by the resistive PCM melt front, the fin structure temperature distribution needs to be adjusted. The derived fin efficiency equations can be seen below in Table 1.

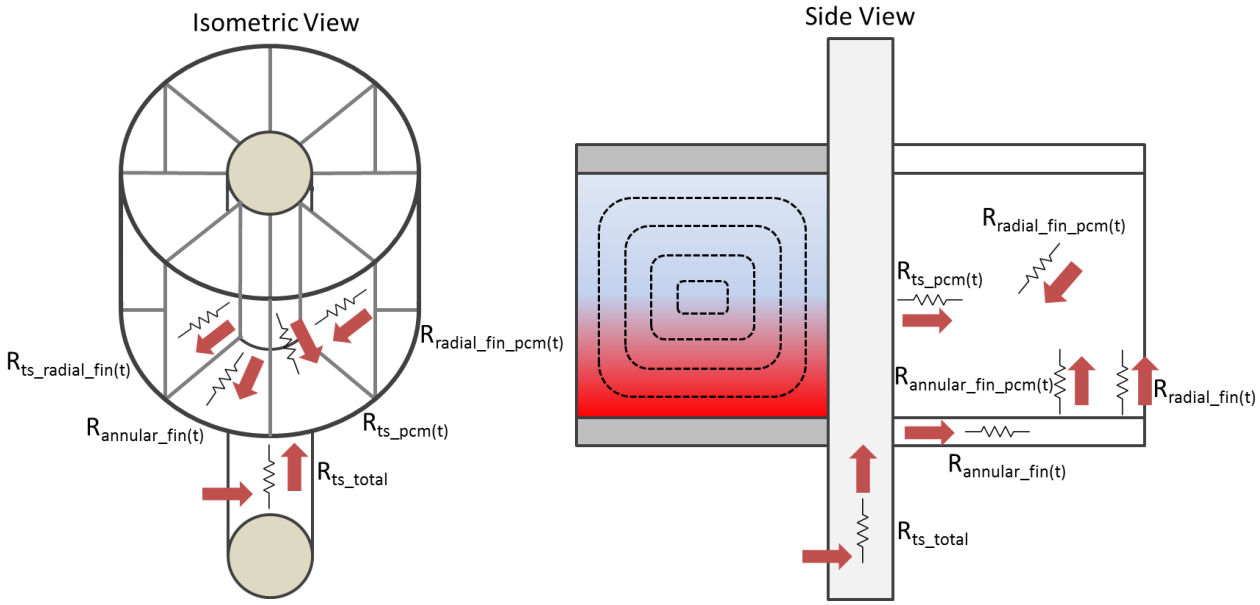

Fig. 5 Isometric and side view of the resistance relationships in the module. An intricate configuration was developed to capture the combined parallel-series resistance network.

Additionally, the transient PCM resistance is accounted for using an energy balance to solve for the changing melt front with each time step. This energy balance is used to calculate the transient numerical solution. An example of the melt front distribution can be seen below in Figure 6. This curve demonstrates that the PCM resistance is accounted for as a function of the melt front propagation. As the PCM melts, a liquid PCM boundary layer develops, which is the dominant resistance pathway [5]. Equation 1 is used to solve for the melt front in the following manner. First, using the specified temperature driving force and equivalent resistance, an initial cooling power is found. The initial temperatures are found using nodal analysis of the resistance network in Figure 3. During the utilization cycle, it is assumed initially that no PCM is melted and there is 100% fin efficiency. Equation 1 is then rearranged to solve for the advancing melt front at the next time step. The changing surface area in contact with PCM is a function of the melt front location. In actuality, there are four differential equations to be solved simultaneously to account for each unique pathway or surface area in contact with PCM [6]. This is demonstrated in Equation 2 for the general form of each rearranged differential equation. Using these results, the specific equivalent resistance can then be found at the next time step. The cycle is repeated until the melt front reaches its geometric constraint. The operational time that this occurs is the melt time of the PCM for a given system configuration [7].

$$q = \frac{d(H\rho V_n)}{dt} = \frac{H\rho A_{s,n}\Delta L_{c,n}}{\Delta t} = \frac{T_{i_n} - T_m}{R_{n,eq}} \tag{1}$$

$$L_{c,n}^{j+1} = L_{c,n}^{j} + \frac{\frac{T_{i_n}^{j} - T_m}{R_{n,eq}^{j}}(t^{j+1} - t^{j})}{H\rho A_{s,n}^{j}} \tag{2}$$

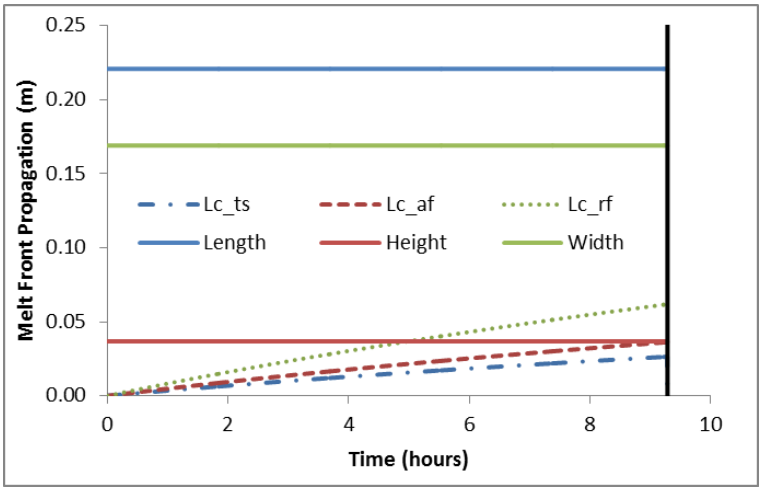

Fig. 6 Example of the three-dimensional melt front propagation during the PCM melting process.

Table 1. Thermal resistances and temperature distributions for the cool storage system

Definition	Equation	Description
Wall Resistance, R_{wall}	$R_w = \frac{\ln(\frac{r_o}{r_i})}{2\pi k_w L_c}$	r_o = heat pipe outer radius, r_i = heat pipe inner radius, k_w = wall conductivity, L_c = characteristic length
Evaporation Resistance, R_e	$R_e = \frac{1}{h_e(2\pi r_i L_e)}$	h_e = evaporative heat transfer coefficient, L_e = evaporator length
Condensation Resistance, R_c	$R_c = \frac{1}{h_c(2\pi r_i L_c)}$	h_c = condensation heat transfer coefficient, L_c = condenser length
Vapor Space Resistance, R_{vs}	$R_{vs} = \frac{T(P_{sat,f}) - T(P_{sat,i})}{q}$	q = cooling power
Annular Fin Temperature Distribution, T_{sf}	$\frac{T(r) - T_m}{T_b - T_m} = \frac{K_1(mR_1)I_0(mr) + I_1(mR_1)K_0(mr)}{K_1(mR_1)I_0(mR_0) + I_1(mR_1)K_0(mR_0)}$	$m^2 = \frac{2k_{pcm}}{k_{fin} \times L_c \times \delta}$
Radial Fin Temperature Distribution, T_{ff}	$\Delta T = (T_b - T_m)(1 - \frac{1}{\cosh(mL_c)})$	T_b = base temperature, T_m = melt temperature
PCM Resistance, R_{pcm}	$R_{pcm} = \frac{L_c}{k_{PCM} A_s}$	k_{pcm} = PCM conductivity, A_s = PCM surface area

3. RESULTS AND DISCUSSION

3.1 Model Validation

The most challenging aspect for accepted use of the TRN Model is to ensure that the thermal performance metrics used are precise with respect to CFD and experimental findings. The modeling derivations were formulated to represent the transient system design using a thermal resistance network. If the comparison is close, then the cost analysis used and integrated with a techno-economic analysis can provide a robust understanding of the market value of the technology and thermal performance drivers. The modeling of the network itself underwent several iterations to precisely define the major thermal resistance pathways. Along the

way, comparisons were made with ANSYS Fluent to ensure the thermal performance (i.e. PCM melt time) was consistent between both modeling techniques. To reiterate, the Excel-based TRN tool is necessary for system parameter sizing and optimization as well as cost analysis. These metrics are paramount from a design standpoint for progression of this project into a realizable product.

The basis of the model validation was founded on the concept that the true thermal performance can be simulated using ANSYS Fluent. Experimental results would then provide a realistic expectation for thermal performance results as another basis of comparison. The TRN Model could be used with confidence following a definitive study of these methods. The results for this type of comparison can be seen below in Figure 7. Results were found using the basic geometric configuration of Figure 4b, which includes radial fin structures inside the module. The sizing was based on an experimental test apparatus. A summary of the results can be seen below in Table 2. The critical takeaways are the overestimation of the PCM melt time with respect to the initial analysis method and the evolution of the modeling technique. Initial analysis using an overall equivalent resistance did not fully capture the physics of the melt front propagation. This is due to the fact that geometric considerations were not taken into account to demonstrate the unique melt front propagation in each dimension. The overall equivalent thermal resistance was used as one term to determine the melt front propagation, which was determined to be inaccurate in matching the physics to CFD. This method becomes unreliable in melt time prediction as the geometric aspect ratios become more drastic. Using the higher fidelity three-dimensional melt front calculation explained above in section 2 on model configuration, the power curve more closely matches the physics seen with doing CFD work. This accounts for the changing fin surface area in contact with PCM as the melting front propagates in each dimension. The heat flux drastically decreases to a constant non-zero value when the PCM is melted completely.

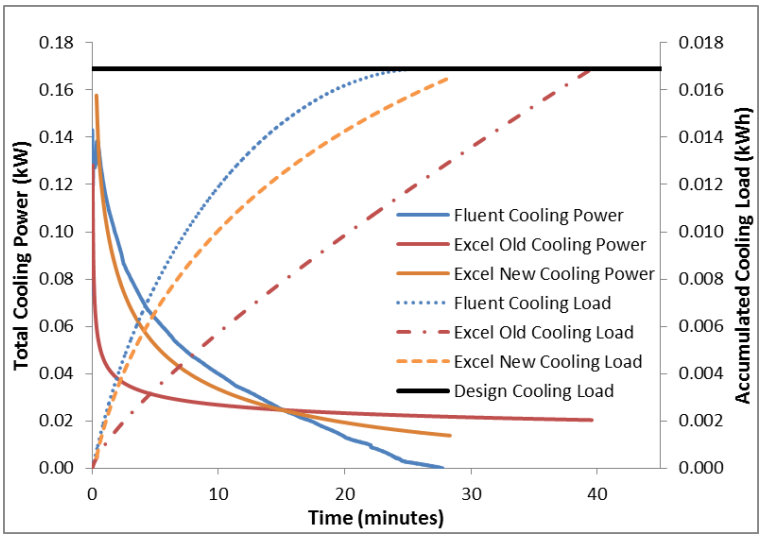

Fig. 7 Subsequent comparison between CFD and Excel TRN modeling methods.

Table 2. Melt time comparison for different analysis methods

	Excel	ANSYS Fluent	Experiment
Melt Time (min.)	28 min.	27 min.	28-32 min.
Analysis Method	Thermal Resistance	CFD	Calorimetry

In addition, a comparative method between thermal resistance and CFD results for PCM analysis is being developed that can predict the appropriate tuning of melt time results. Using thermal resistance calculations is computationally less intensive than robust CFD equations. The idea here is to develop a characteristic curve that can demonstrate how the melt time results using thermal resistance calculations can be tuned to the true value found in CFD for any geometric configuration. This fundamental concept can then be applied to the results of the TRN to ensure that the thermal performance of the system is precise. To determine this

analysis correctly, this concept was first applied to estimating the melt time of a rectangular slab of PCM. As shown in Figure 8, the model has an appropriate wall temperature on two sides and zero heat flux on the other sides. The ten cases shown below in Table 3 were tested. The temperature difference between the wall and melting temperature was fixed at 10°C and the thermal conductivity was set to 0.5 W/m-K. Figure 9 below demonstrates the results for this comparison. There is a clear overestimation of the melt time results using thermal resistance calculations compared to CFD. A characteristic tuning curve can be created based on these initial results to test the prediction capabilities of using thermal resistance calculations to demonstrate thermal performance for any given case study.

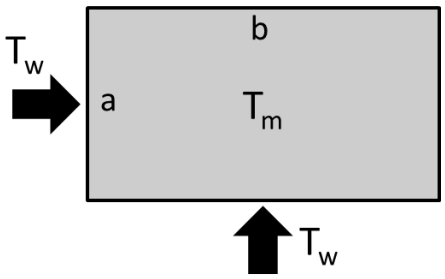

Fig. 8 A two-dimensional representation of PCM.

Table 3. Initial test cases used in two-dimensional analysis to form characteristic curve

Case	1	2	3	4	5	6	7	8	9	10
a (cm)	0.1	0.3	0.5	1	1.5	2	2.5	3	3.5	4
b (cm)	4	4	4	4	4	4	4	4	4	4
Ratio (a:b)	0.025	0.075	0.125	0.25	0.375	0.50	0.625	0.75	0.875	1

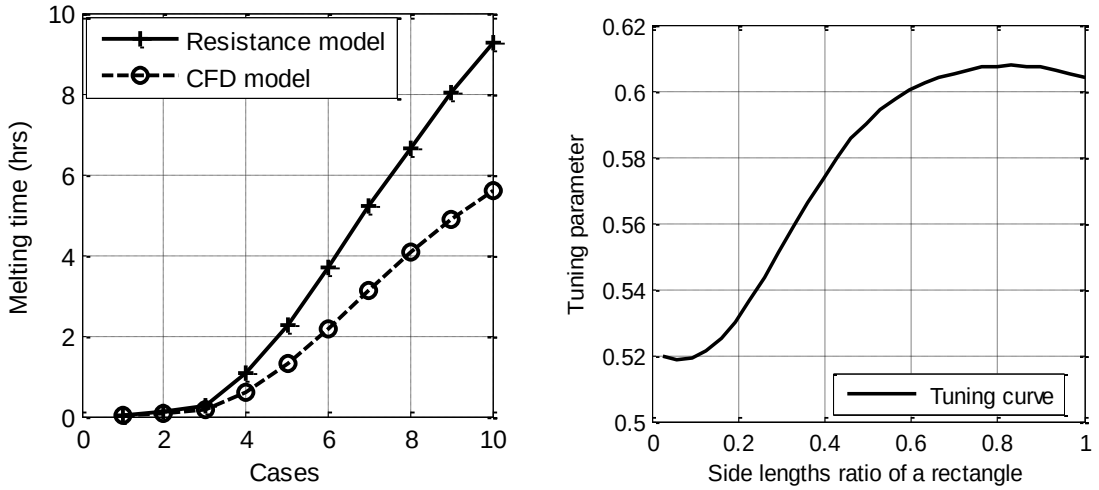

Fig. 9 The melt time results (left) and characteristic curve (right) for the resistance and CFD model. The characteristic curve demonstrates a scaling factor for resistance calculations.

Now with a characteristic curve, a tuning parameter can be used with the thermal resistance analysis method to demonstrate its prediction ability for different design cases. Table 4 contains ten new test cases used with varying length ratios, driving temperature, and PCM thermal conductivity. The performance of this analysis is shown below in Figure 10. Overall, the prediction accuracy is quite high with a typical error less than 3%. The error is associated between the scaled resistance results and the CFD results for the new design cases. To test the flexibility in this modeling approach, different values for the driving temperature difference and PCM thermal conductivity are used in test cases. The expectation is that a characteristic curve for a comparable

geometry to that of the proposed technology for any design condition can be used for the thermal resistance calculations in the TRN. To address the noted error in the technique, it is theorized that the reducing area of PCM in contact with the boundary contributes to a geometrical inaccuracy in the calculations. In other words, the resistance calculations oversimplify the changing geometry of PCM during the phase change process. Further work is being done to attribute this model to a three-dimensional structure for a more detailed approach.

Table 4. Ten new test cases to validate the tuning parameters of the characteristic curve

Case	1	2	3	4	5	6	7	8	9	10
ΔT (°C)	10	10	10	15	20	7	10	10	20	50
k_{pcm} W/m-K	0.5	0.5	0.5	0.5	0.5	0.5	1	0.3	2.0	0.5
a (cm)	1	3	5	3	3	1	3	1	5	6
b (cm)	5	5	5	5	5	5	5	5	6	6
Ratio (a:b)	0.2	0.6	1	0.6	0.6	0.2	0.6	0.2	0.83	1

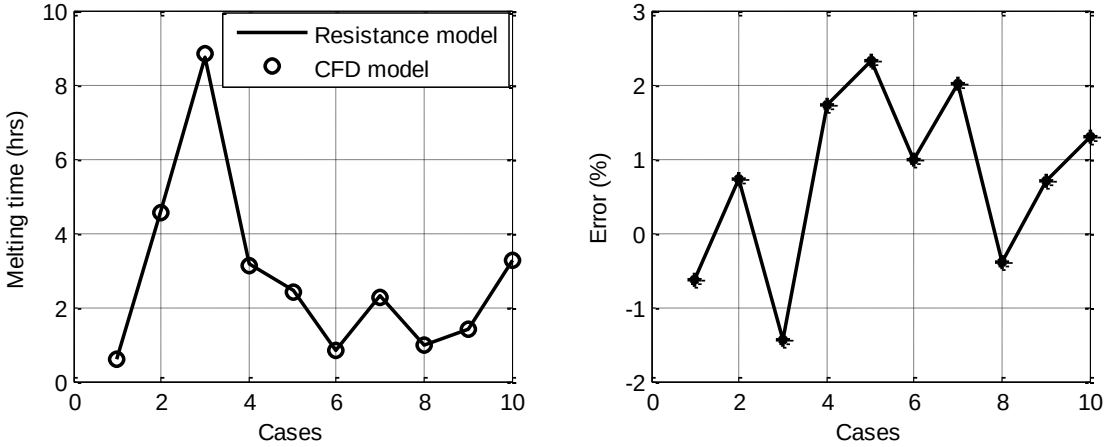

Fig. 10 Thermal performance results after using the tuning capabilities of the characteristic curve.

3.2 Parametric Studies

Optimization of the cool storage system is challenging based on the variety of design parameters used to determine the thermal performance, system sizing, and overall capital cost. To analyze the system with varying design input parameters, it is important to establish an analysis process. This will help determine how to optimize the component design parameters with respect to thermal performance and capital cost. The design analysis process can be seen below in Figure 11. The first step is to specify the various design input parameters. Specifically, this includes initial and boundary conditions, material selection, and system sizing. The second step involves using the numerical model configuration to solve for the component transient thermal resistances and changes in temperature. Following this in step three, operational curves can be developed to demonstrate the melt capabilities and cost analysis of the current system design. In step four, the current design is analyzed to determine if the thermal performance and capital cost capabilities are met. For thermal performance, a typical metric used is if the PCM melted within the given time constraint. In the case of a power plant application, this value would be a 10 hour operational limit. Another metric from the program goals is to design a system that has less than a 5°C temperature drop from the thermosyphon outer wall to the PCM interface. For the cost analysis, it is paramount that the overall capital cost of the system can be demonstrated to be less than $\$150/kW_{th}$. This metric was established by the ARPA-e program as a guideline for reasonable market penetration for the technology. If the current design does not meet any one of these goals, step 4b specifies that the design input parameters must be altered. This is where the optimization aspect of the project is critical. With an understanding of how each input parameter affects the overall thermal performance and capital cost of the system, more reasonable choices can be made to work towards a better design. If the design goals are met, the analysis is complete and subsequent results can be used towards production.

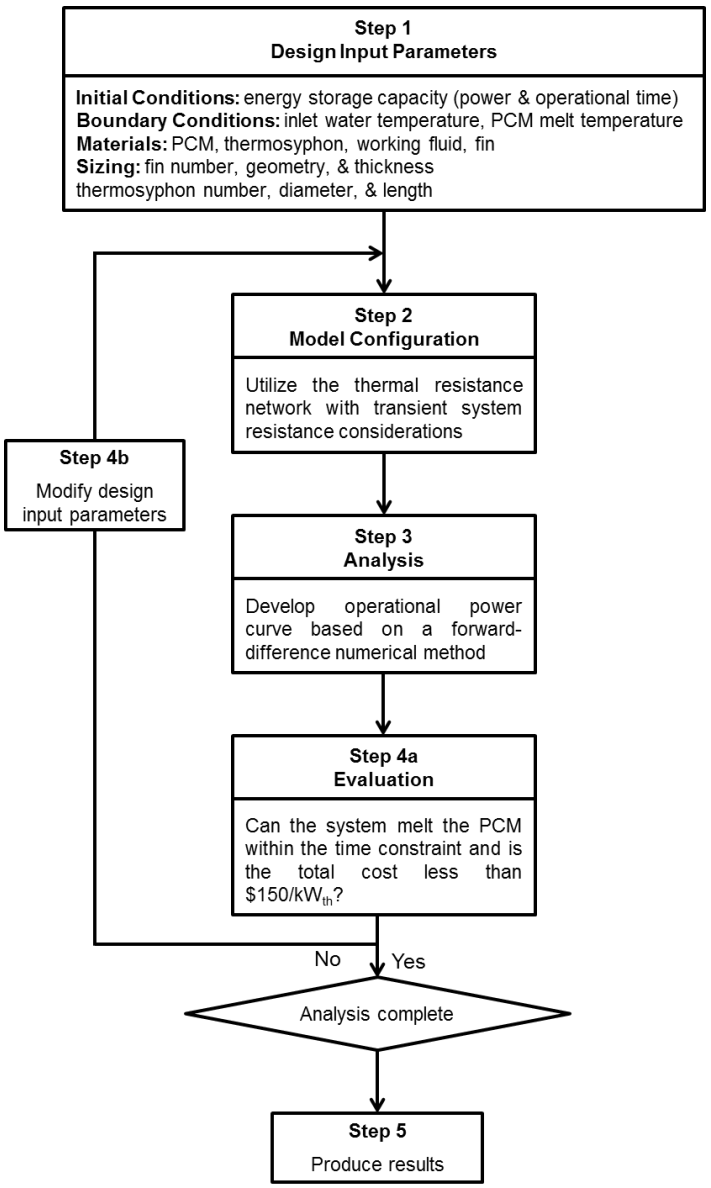

Fig. 11 Design analysis sequence for the modeling process [8].

An example of an important system analysis can be seen by varying the annular fin pitch, or in other words, the axial spacing between each module. To meet the thermal performance and capital cost goals, a multitude of parametric studies will be done to understand how to tune the various input parameters. This is one example of this analysis. This analysis is completed by varying one parameter for each iteration of the design sequence while all other input parameters are held constant. It is also important to note that the results do not necessarily represent an optimum system; rather, they represent a possible solution that can meet the design constraints. Ultimately, a local optimum can only be found after many iterative studies for a specific design case. In Figure 12 and Figure 13, it is demonstrated how changing the number of thermosyphons affects the total capital cost and temperature drive through the system, respectively. This is done while varying the annular fin pitch to understand a potential range of sizing. The number of thermosyphons is varied due to the fact that it influences the module sizing calculations for a given amount of PCM. It is clear from both figures that there is a "breaking point" in which using too many thermosyphons negatively affects the outcome. Another result of this analysis demonstrates that a large enough fins per inch (fpi) is necessary to ensure a system temperature drop within the design goal. Too large of a module height limits the efficient melting capabilities of the PCM. This can be compared against the cost analysis to develop an approximate range (purple area) for these input parameters. Subsequent studies will delve into a complete system analysis for all input parameters.

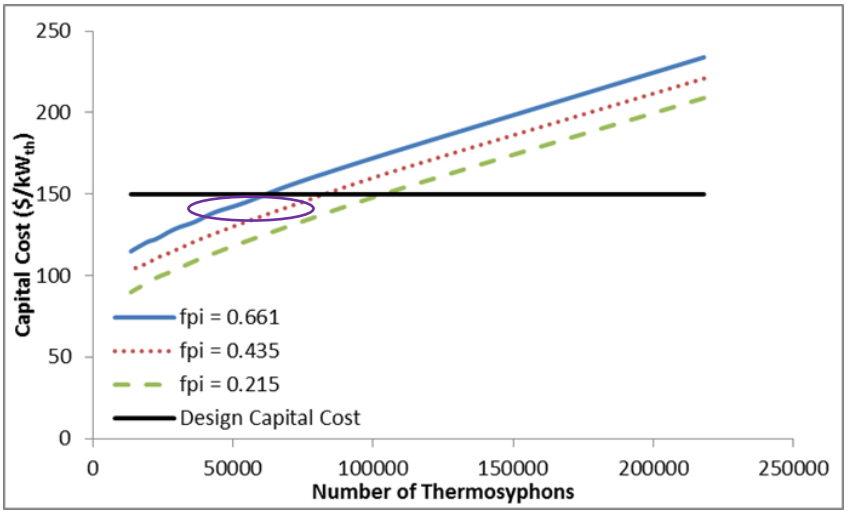

Fig. 12 Influence of capital cost versus number of thermosyphons at varying annular fin spacing.

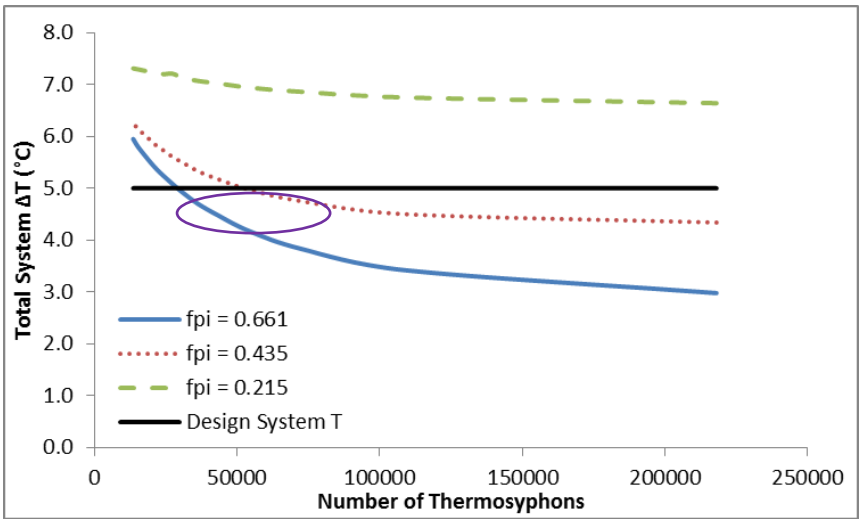

Fig. 13 Influence of total ΔT versus the number of thermosyphons at varying annular fin spacing.

Another parametric study of interest involves the investigation of thermosyphon diameter sizing. For an arbitrary system sizing, the trend of how thermosyphon diameter sizing affects overall thermal performance and capital cost was studied. The results of this study are seen below in Figure 14 and Figure 15. In Figure 14, it was analyzed how the capital cost of the system changes with a different number of thermosyphons while varying the nominal pipe sizing (NPS) of the thermosyphon. It is clear from the graph that the change in capital cost is small and insignificant with varying thermosyphon diameter at a constant number of thermosyphons. Although the cost is typically above \$150/kW$_{th}$, this can be adjusted. It is the trend in data that dictates the optimization, as the magnitude for the variable of interest can always be adjusted through optimization of other design input parameters. It is understood that although the design input parameters are dependent on each other, this type of assessment can guide the design study to determine an option that will meet the design goals. In Figure 15, the thermal performance is compared using the same metrics. This analysis reveals that there are diminishing returns to increasing the thermosyphon diameter to achieve a lower melt time. This is due to the fact that at larger diameter thermosyphons, there is a decreased thermal resistance in the thermosyphon itself for comparable conditions. A higher heat flux can then be achieved, which results in a shorter melt time. In summary, these results demonstrate the need for large diameter thermosyphons using the least number of thermosyphons possible for a given operational time. This insight will help to determine the optimization of other design input parameters knowing that the thermosyphon diameter can be tuned to an appropriate melt time.

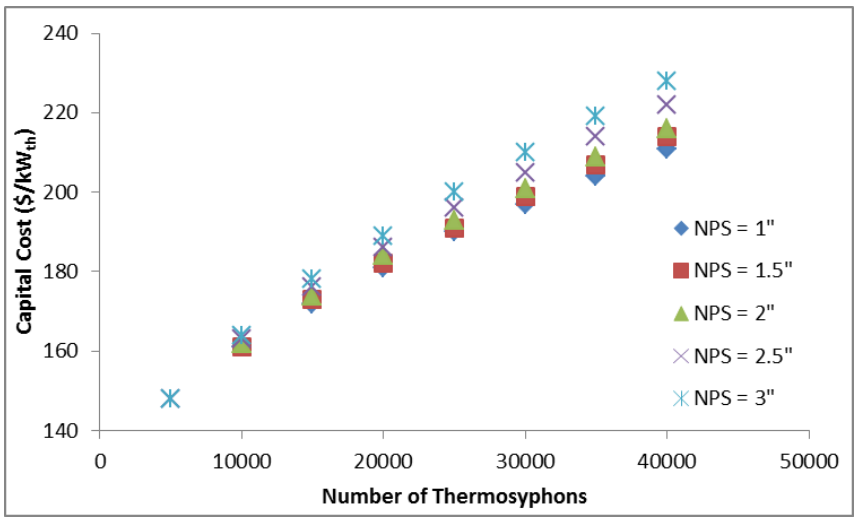

Fig. 14 Influence of capital cost versus number of thermosyphons at varying diameter sizing.

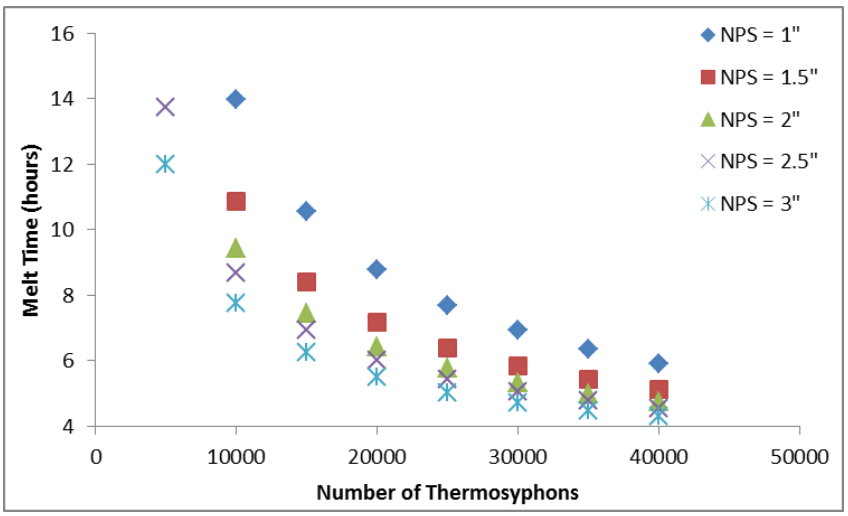

Fig. 15 Influence of melt time versus number of thermosyphons at varying diameter sizing.

4. CONCLUSIONS

To properly simulate the thermal performance and capital cost of this cool storage technology is paramount to its successful progression. In this work, it is demonstrated that a numerical Excel-based thermal resistance network can achieve these goals. A complex mathematical model was built to account for the fundamental heat transfer physics associated with the cool storage system. This included a unique three-dimensional melt front propagation construct to precisely capture the system thermal performance. Validation with ANSYS Fluent was used to ensure precise simulation of the PCM phase change process. Further progression of these higher fidelity methods will ensure accurate representation of this phenomenon. Parametric studies were completed to understand the optimum trends in the design input parameters. Continued efforts will demonstrate a holistic understanding of the system design. To capture the technology's value in the market, a more complete techno-economic analysis is being done using the results of the model. With the knowledge gained from the use of this network, a more complete optimal design can be produced within the thermal performance and capital cost goals. It is clear from the results demonstrated thus far that a PCM heat exchanger system for power plant applications is viable within the given cost and thermal constraints of \$150/kW_{th} and 10 hour operational time, respectively. The developed thermal resistance network model will guide the design of future prototypes to demonstrate the theoretical and practical feasibility of this heat pipe-PCM cool storage system.

ACKNOWLEDGMENT

This research is sponsored by the ARPA-e ARID Program under Contract No. DE-AR0000582. Any opinions, findings, and conclusions or recommendations expressed in this article are those of the authors and do not necessarily reflect the views of the Advanced Research Projects Agency-Energy. Dr. Michael Ohadi is the current ARPA-e ARID Program Manager.

NOMENCLATURE

H	Latent heat of fusion	(J/kg)	L_c	Characteristic length	(m)
T_i	Initial Temperature	(°C)	T_m	Melt Temperature	(°C)
T_{fin}	Fin Temperature	(°C)	T_{wall}	Condenser Wall Temperature	(°C)
j	Present time step	(-)	$j+1$	Future time step	(-)
n	Arbitrary geometric dimension	(-)	i_n	Arbitrary inlet temperature	(-)

REFERENCES

[1] *ARPA-e ARID Program Overview*. Retrieved September 09, 2016 from http://arpa-e.energy.gov/, (2014).
[2] U.S. Department of Energy., *The Water-Energy Nexus: Challenges and Opportunities*. Retrieved September 09, 2016 from http://www.energy.gov/, (2014).
[3] Yaffee, S. and et. al. *Renewable Energy in the California Desert*. Retrieved September 12, 2016 from http://webservices.itcs.umich.edu/, (2010).
[4] Tay, N.H.S., M. Belusko, A. Castell, L.F. Cabeza, and F. Bruno, "An Effectiveness-NTU Technique for Characterizing a Finned Tubes PCM System using a CFD Model." *Applied Energy* 131 (2014): 377-385.
[5] Zheng, Y., J.L. Barton, K. Tuzla, J.C. Chen, S. Neti, A. Oztekin, and W.Z. Misiolek, "Experimental and Computational Study of Thermal Energy Storage with Encapsulated $NaNO_3$ for High Temperature Applications." *Solar Energy* 115 (2015): 180-194.
[6] Tay, N.H.S., M. Belusko, and F. Bruno, "An Effectiveness-NTU Technique for Characterizing Tube-in-Tank Phase Change Thermal Energy Storage Systems." *Applied Energy* 91 (2012): 309-319.
[7] Zhao, W., Y. Zheng, J.C. Chen, and et. al., "Heat Transfer Analysis for Thermal Energy Storage Using $NaNO_3$ as Encapsulated Phase Change Material." *ASME Summer Heat Transfer Conference* (2012).
[8] Weng, Y.C, H.P. Cho, C.C. Chang, and S.L. Chen, "Heat Pipe with PCM for Electronic Cooling." *Applied Energy* 88 (2011): 1825-1833.